Optimizing single microwave-photon detection: Input-Output theory

M. Schöndorf,[1] L. C. G. Govia,[1,*] M. Vavilov,[2] R. McDermott,[2] and F. K. Wilhelm[1]

[1] *Theoretical Physics, Saarland University, 66123 Saarbrücken, Germany*
[2] *Department of Physics, University of Wisconsin-Madison, Madison, WI 53706, USA*

High fidelity microwave photon counting is an important tool for various areas from background radiation analysis in astronomy to the implementation of circuit QED architectures for the realization of a scalable quantum information processor. In this work we describe a microwave photon counter coupled to a semi-infinite transmission line. We employ input-output theory to examine a continuously driven transmission line as well as traveling photon wave packets. Using analytic and numerical methods, we calculate the conditions on the system parameters necessary to optimize measurement and achieve high detection efficiency.

I. INTRODUCTION

Circuit quantum electrodynamics (cQED) has emerged as a powerful paradigm for the realization of quantum computational circuits in a scalable architecture [1–5] as well as a demonstration of quantum radiation-matter interaction in the strong and ultra strong coupling regimes [6–9]. Here, the two lowest energy levels of a superconducting Josephson circuit play the role of an artificial atom, while thin film cavities and transmission lines are used to realize electromagnetic field modes. Strong coupling between the cavity fields and the artificial atom has been used to create strongly non classical states of the electromagnetic field [7, 10–14]; in addition, coupling between these modes and the Josephson circuit can be used for high fidelity control [15, 16] and measurement [17–26].

In conventional, optical-frequency implementations of quantum optics, detection of the electromagnetic mode is performed by a photon counter. The counter is typically modeled as an ensemble of two-level states that are weakly coupled to the light field [27]. Photon absorption is accompanied by generation of a large, easily measured classical signal, and detector performance is expressed in terms of quantum efficiency and spurious dark count rate [28]. In the microwave frequency range, conventional wisdom holds that there exists no material that can be photoionized by the lower frequency radiation. However, a variety of Josephson circuits are capable of detecting single microwave photons with high efficiency [29–37]. In contrast to optical-frequency counters, Josephson-based microwave photon counters are realized as single effective two-level systems that couple strongly to the incident microwave field [29]. For this reason, they differ fundamentally from optical frequency counters. It is the purpose of this paper to explore the conditions for high-efficiency detection of propagating photons by these single, strongly coupled Josephson circuits. For the sake of completeness, we consider the Josephson photomultiplier (JPM), a current-biased junction capable of efficient detection of microwaves that are near resonant with the transition between the two lowest states in the metastable minima of the circuit potential. Previously, the JPM has been applied to investigation of temporal correlations of incident coherent and thermal microwave fields [30], and the JPM is currently under investigation for high fidelity measurement of single qubits [38] and of multiqubit parity operators [39]. Other approaches to single microwave photon detection include driven Λ systems [40]. In this approach, the dressed states of a qubit-resonator system constitute an impedance-matched system, which absorbs an input photon with a near-unity efficiency [41, 42].

Here, we demonstrate that efficient microwave photon detection can be understood from a simple intuitive picture of rate matching, which has as its classical analog the usual impedance matching condition that provides for optimal power transfer in microwave circuits [43]. We present a general description of a transmission line directly coupled to a JPM, and explore the conditions that must be met to maximize detector quantum efficiency. Our results agree with those of [44], where only a continuous drive input state was considered. Furthermore, our results extend beyond those of [44] as we include additional incoherent channels and study pulsed input states.

To describe our system, we use input-output formalism [45, 46], a tool from the field of open quantum systems theory, that leads to generalized Heisenberg equations. The advantage of this approach is that it does not require us to specify the form of the photon pulse in the transmission line. As a result, we can examine arbitrary states in the transmission line, including both continuous wave drive and wave packets with finite photon number.

The input-output formalism leads to a system of equations,from which we determine conditions on the system parameters that allow us to optimize detection efficiency. A sufficient set of these parameters can be designed or even controlled in experiment such that this paper provides a guide towards practical implementation of the measurement of traveling photons using a JPM, achieving the optimal measurement efficiency experimentally possible.

This paper is organized as follows. In Sec. II, we present the system of interest and derive the corresponding equations of motion using input-output formalism. In

* Current Address: Departement of Physics, McGill University, Montreal, Quebec, Canada H3A 2T8

Sec. III, we solve the resulting equations by substituting operators with their corresponding expectation values. This simplification leads to rate equations, the solution of which yields to a general matching condition for measurement optimization. In Sec. IV, we we use a mean field approach that captures more of the quantum mechanical character of the system. We find the optimization conditions for continuous drive inputs, and for various pulsed waveforms. In Sec. V, we present our conclusions.

II. SYSTEM AND EQUATIONS OF MOTION

The system of interest is a microwave transmission line directly coupled to a JPM. The system Hamiltonian is written as

$$\hat{H} = \hat{H}_{\mathrm{JPM}} + \hat{H}_{\mathrm{TL}} + \hat{H}_{\mathrm{INT}}, \tag{1}$$

where $\hat{H}_{\mathrm{JPM}}$ denotes the Hamiltonian of the JPM, $\hat{H}_{\mathrm{TL}}$ is the bare transmission line Hamiltonian, and $\hat{H}_{\mathrm{INT}}$ describes the interaction between the transmission line and the JPM. The JPM is realized through a current biased Josephson junction and is described by a tilted washboard potential [47], from which one can isolate two quasi-bound energy levels $|0\rangle$ and $|1\rangle$, with associated Hamiltonian

$$\hat{H}_{\mathrm{JPM}} = -\hbar\omega_0 \frac{\hat{\sigma}_z}{2}. \tag{2}$$

Here, ω_0 is the transition frequency and $\hat{\sigma}_z = \left[\hat{\sigma}, \hat{\sigma}^\dagger\right]$ is the usual Pauli-Z operator with

$$\hat{\sigma} = |0\rangle\langle 1| \qquad \hat{\sigma}^\dagger = |1\rangle\langle 0|. \tag{3}$$

Note that the local minima in the JPM potential are physically equivalent and only transitions between them can be detected [48] (see Fig. 1). Both states can tunnel to the continuum with rate γ_0 and γ_1, respectively. For our description, we represent the continuum by a fictitious measurement state $|m\rangle$. Incoherent tunneling to the $|m\rangle$ state corresponds to generation of a measurable voltage pulse. Absorption of a resonant photon induces a transition from $|0\rangle$ to $|1\rangle$, which tunnels rapidly to the continuum since $\gamma_1 \gg \gamma_0$; this system can thus be used to count incoming photons.

Quantization of the transmission line [17] leads to the usual multimode harmonic oscillator Hamiltonian:

$$\hat{H}_{\mathrm{TL}} = \hbar \int_0^\infty \omega \hat{a}^\dagger(\omega)\hat{a}(\omega)\mathrm{d}\omega. \tag{4}$$

Here, ω is the frequency of the transmission line mode and $\hat{a}^\dagger(\omega)$, $\hat{a}(\omega)$ are the bosonic creation and annihilation operators for a photon at frequency ω, respectively. Note that the density of modes is included in $\hat{a}(\omega)^\dagger$ and $\hat{a}(\omega)$. As a result we have $\hat{a}^\dagger(\omega) = f(\omega)\hat{a}^\dagger(\omega)$, where $f(\omega)$ is the envelope of the incoming radiation in frequency space. The interaction between the JPM and the transmission line arises from the additional bias on the JPM caused by the transmission line current (see Fig. 1). This leads to a dipole interaction between the JPM states and the transmission line described by the Hamiltonian

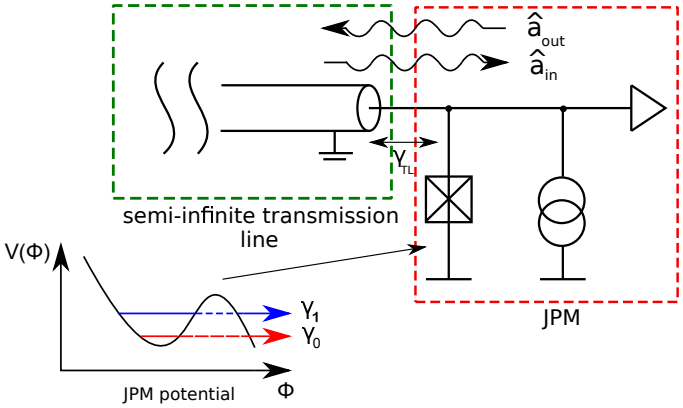

FIG. 1. System schematic. The JPM is directly coupled to a transmission line which excites the JPM by an incoming photon flux. The potential of the JPM is a tilted washboard with two quasi-bound states in the local minima.

$$\hat{H}_{\mathrm{INT}} = \Delta\hat{I}\frac{\Phi_0}{2\pi}\hat{\varphi}_J, \tag{5}$$

where $\Phi_0 \equiv h/2e$ is the magnetic flux quantum and $\Delta\hat{I}$ and $\hat{\varphi}_J$ describe the additional quantized current coming from the transmission line and the quantized phase of the JPM, respectively. To derive expressions for $\Delta\hat{I}$ and $\hat{\varphi}_J$ we use standard circuit quantization, which yields [49, 50]

$$\Delta\hat{I} = \sqrt{\frac{\hbar\omega_s}{4\pi Z_0}}\int_0^\infty \mathrm{d}\omega\left(\hat{a}^\dagger(\omega) + \hat{a}(\omega)\right) \tag{6}$$

$$\hat{\varphi}_J = \frac{i}{\sqrt{2}}\left(\frac{2E_C}{E_J}\right)^{\frac{1}{4}}\left(\hat{\sigma}^\dagger - \hat{\sigma}\right). \tag{7}$$

Here Z_0 is the transmission line impedance; ω_s is the characteristic signal frequency; $E_C = (2e)^2/2C_J$ is the Cooper pair charging energy, with the junction self-capacitance C_J; and $E_J = \hbar I_c/2e$ is the Josephson coupling energy, where I_c is the critical current of the junction. Inserting expressions (6) and (7) into (5), we obtain the quantized interaction Hamiltonian

$$\hat{H}_{\mathrm{INT}} = i\hbar\underbrace{\sqrt{\frac{\omega_s Z_J}{8\pi Z_0}}}_{\equiv\sqrt{\gamma_{\mathrm{TL}}/2\pi}}\int_{-\infty}^{\infty}\mathrm{d}\omega\left[\hat{a}^\dagger(\omega)\hat{\sigma} - \hat{\sigma}^\dagger\hat{a}(\omega)\right], \tag{8}$$

where γ_{TL} describes the coupling rate between the transmission line and the JPM. The expression for γ_{TL} includes the junction impedance $Z_J = 1/\omega_s C_J$.

For this derivation (see Appendix A) we applied the rotating-wave-approximation (RWA) [51], which leads to a continuous Jaynes-Cummings interaction [52] and allows us to put the lower limit of integration to $-\infty$ in-

stead of 0. We further assumed that the coupling is constant over all modes, which is the first Markov approximation [53]. Since the interaction is described by (8), we can use standard input-output formalism [45] to derive the quantum mechanical Langevin equation for an arbitrary JPM operator $\hat{S}$

$$\begin{aligned}\dot{\hat{S}}(t) = &\frac{i}{\hbar}\left[\hat{H}_{\mathrm{JPM}}, \hat{S}(t)\right] \\ &- \left[\hat{S}(t), \hat{\sigma}^\dagger(t)\right]\left\{\frac{\gamma_{\mathrm{TL}}}{2}\hat{\sigma}(t) - \sqrt{\gamma_{\mathrm{TL}}}\hat{a}_{\mathrm{in}}(t)\right\} \\ &+ \left\{\frac{\gamma_{\mathrm{TL}}}{2}\hat{\sigma}^\dagger(t) - \sqrt{\gamma_{\mathrm{TL}}}\hat{a}^\dagger_{\mathrm{in}}(t)\right\}\left[\hat{S}(t), \hat{\sigma}(t)\right],\end{aligned} \tag{9}$$

with input field operator defined as

$$\hat{a}_{\mathrm{in}}(t) \equiv -\frac{i}{\sqrt{2\pi}}\int_{-\infty}^{\infty} \mathrm{d}\omega \exp\left[-i\omega\left(t - t_0\right)\right]\hat{a}_{t_0}(\omega), \tag{10}$$

where $\hat{a}_{t_0}(\omega)$ is the field operator at time $t = t_0$. Without loss of generality, we set the starting point of the interaction to zero, $t_0 = 0$. Our system satisfies the standard input-output relation [51]

$$\hat{a}_{\mathrm{out}}(t) + \hat{a}_{\mathrm{in}}(t) = \sqrt{\gamma_{\mathrm{TL}}}\hat{\sigma}(t), \tag{11}$$

where the output field operator is defined as

$$\hat{a}_{\mathrm{out}}(t) = \frac{i}{\sqrt{2\pi}}\int_{-\infty}^{\infty} \exp\left[-i\left(t - t_1\right)\right]\hat{a}_{t_1}(\omega). \tag{12}$$

Here, $\hat{a}_{t_1}(\omega)$ is similar to $\hat{a}_{t_0}(\omega)$ in that it is defined as the field operator at a time $t_1 > t_0$ after the interaction between transmission line and JPM is turned on.

Up to now we have not considered incoherent channels of the JPM. We include them using the standard Lindblad formalism. The Lindblad operator that describes tunneling from the excited state to the continuum (measurement process) is

$$\hat{L}_1 = \sqrt{\gamma_1}\left|m\right\rangle\left\langle 1\right|, \tag{13}$$

with tunneling rate γ_1, where the state $|m\rangle$ represents all states outside the potential well of the quasi-bound states. Another incoherent channel is given by dark counts

$$\hat{L}_0 = \sqrt{\gamma_0}\left|m\right\rangle\left\langle 0\right|, \tag{14}$$

a tunneling with rate γ_0 from the ground state of the JPM into the measurement state. We also take into account the possibility of relaxation from $|1\rangle$ to $|0\rangle$ through energy loss to the environment. This process is represented by the Lindblad operator

$$\hat{L}_{\mathrm{rel}} = \sqrt{\gamma_{\mathrm{rel}}}\left|0\right\rangle\left\langle 1\right|, \tag{15}$$

where γ_{rel} is the relaxation rate. This rate only includes emission into the intrinsic environment of the JPM, since emission back to the transmission line is already built into the input-output equations. Finally, we assume that the JPM has the possibility to reset after a measurement, such that multiple measurements are possible. The reset is described by the operator

$$\hat{L}_{\mathrm{res}} = \sqrt{\gamma_{\mathrm{res}}}\left|0\right\rangle\left\langle m\right|, \tag{16}$$

where γ_{res} is the reset rate. The reset process brings the JPM from the measurement state $|m\rangle$ back to the ground state $|0\rangle$.

To include these Lindblad channels in the above Langevin equation, we use the adjoint master equation [54]

$$\begin{aligned}\dot{\hat{S}}(t) = &\frac{i}{\hbar}\left[H_{\mathrm{JPM}}, \hat{S}(t)\right] \\ &+ \sum_k\left(\hat{L}_k^\dagger S(t)\hat{L}_k - \frac{1}{2}\hat{S}(t)\hat{L}_k^\dagger\hat{L}_k - \frac{1}{2}\hat{L}_k^\dagger\hat{L}_k\hat{S}(t)\right),\end{aligned} \tag{17}$$

with $k \in \{0, 1, \mathrm{rel}, \mathrm{res}\}$. Combining (9) and (17), we obtain a Langevin-Lindblad master equation that describes the coherent and incoherent dynamics of an arbitrary system operator

$$\begin{aligned}\dot{\hat{S}}(t) = &\frac{i}{\hbar}\left[\hat{H}_{\mathrm{JPM}}, \hat{S}(t)\right] \\ &- \left[\hat{S}(t), \hat{\sigma}^\dagger(t)\right]\left\{\frac{\gamma_{\mathrm{TL}}}{2}\hat{\sigma}(t) - \sqrt{\gamma_{\mathrm{TL}}}\hat{a}_{\mathrm{in}}(t)\right\} \\ &+ \left\{\frac{\gamma_{\mathrm{TL}}}{2}\hat{\sigma}^\dagger(t) - \sqrt{\gamma_{\mathrm{TL}}}\hat{a}^\dagger_{\mathrm{in}}(t)\right\}\left[\hat{S}(t), \hat{\sigma}(t)\right] \\ &+ \sum_k\left(\hat{L}_k^\dagger S(t)\hat{L}_k - \frac{1}{2}\left[\hat{S}(t)\hat{L}_k^\dagger\hat{L}_k + \hat{L}_k^\dagger\hat{L}_k\hat{S}(t)\right]\right).\end{aligned} \tag{18}$$

All of the above Lindblad operators describe loss channels of the JPM. In general, the transmission line can also evolve incoherently; however, the rates for these processes are slow compared to JPM processes [55],[56], so they are ignored in our calculations.

We are interested in the occupation probabilities of the different JPM states, defined by the projection operators

$$\hat{\mathcal{P}}_0 \equiv \left|0\right\rangle\left\langle 0\right| \qquad \hat{\mathcal{P}}_1 \equiv \left|1\right\rangle\left\langle 1\right| \qquad \hat{\mathcal{P}}_m \equiv \left|m\right\rangle\left\langle m\right|. \tag{19}$$

To obtain a complete system of equations, we must also include the system raising and lowering operators $\hat{\sigma}$, $\hat{\sigma}^\dagger$. Putting these five operators into equation (18) leads to a set of coupled ordinary differential equations

$$\dot{\hat{\sigma}} = -i\omega_0\hat{\sigma} + \sqrt{\gamma_{\mathrm{TL}}}\hat{\sigma}_z\hat{a}_{\mathrm{in}} - \frac{\tilde{\gamma}}{2}\hat{\sigma} \tag{20a}$$

$$\dot{\hat{\sigma}}^\dagger = i\omega_0\hat{\sigma}^\dagger + \sqrt{\gamma_{\mathrm{TL}}}\hat{a}^\dagger_{\mathrm{in}}\hat{\sigma}_z - \frac{\tilde{\gamma}}{2}\hat{\sigma}^\dagger \tag{20b}$$

$$\dot{\hat{\mathcal{P}}}_0 = -\gamma_0\hat{\mathcal{P}}_0 + (\gamma_{\mathrm{TL}} + \gamma_{\mathrm{rel}})\hat{\mathcal{P}}_1 - \sqrt{\gamma_{\mathrm{TL}}}\hat{\mathcal{W}} + \gamma_{\mathrm{res}}\hat{\mathcal{P}}_m \tag{20c}$$

$$\dot{\hat{\mathcal{P}}}_1 = -(\gamma_{\mathrm{TL}} + \gamma_{\mathrm{rel}} + \gamma_1)\hat{\mathcal{P}}_1 + \sqrt{\gamma_{\mathrm{TL}}}\hat{\mathcal{W}} \tag{20d}$$

$$\dot{\hat{\mathcal{P}}}_m = \gamma_0\hat{\mathcal{P}}_0 + \gamma_1\hat{\mathcal{P}}_1 - \gamma_{\mathrm{res}}\hat{\mathcal{P}}_m, \tag{20e}$$

where $\tilde{\gamma}$ is defined as $\tilde{\gamma} \equiv \gamma_{\mathrm{TL}} + \gamma_0 + \gamma_1 + \gamma_{\mathrm{rel}}$ and $\hat{\mathcal{W}} \equiv \hat{a}_{\mathrm{in}}^\dagger \hat{\sigma} + \hat{\sigma}^\dagger \hat{a}_{\mathrm{in}}$. All operators are time-dependent, since we are in the Heisenberg picture. Here and in the following, however, we will only indicate this time dependence explicitly when it is necessary for clarity.

It should be noted that up to this point we have made no assumptions about the input field $\hat{a}_{\mathrm{in}}$, such that the derived system of equations describes a completely general situation. This allows us to examine different incoming fields in the cavity, including both continuous drive and various forms of pulses.

III. RATE EQUATIONS

In this section, we approximate equations (20a)-(20e) and find optimization conditions to maximize measurement efficiency in the stationary state. To simplify the system of equations, we substitute for the operator $\hat{\sigma}_z$ its expectation value

$$\sigma_z(t) \longmapsto \langle \sigma_z(t) \rangle = P_0(t) - P_1(t), \tag{21}$$

where P_0 and P_1 denote the probability to be in the ground and excited state, respectively. We want to study a continuous resonant drive $\omega_s = \omega_0$, such that

$$\hat{a}_{t_0}(\omega) = \hat{a}_{t_0} \sqrt{\omega_0} \delta(\omega - \omega_0), \tag{22}$$

since a single mode drive is described by a δ-function in frequency space (for more detail on how to model incoming radiation fields in the Heisenberg picture see [57]). In this case, the Fourier transformation of (20a) can easily be done:

$$\begin{aligned} -i\omega_0 \hat{\sigma}(\omega_0) = &- \left(i\omega_0 + \frac{\tilde{\gamma}}{2} \right) \hat{\sigma}(\omega_0) \\ &+ \sqrt{\gamma_{\mathrm{TL}}} \hat{a}_{\mathrm{in}}(\omega_0)(P_0(\omega_0) - P_1(\omega_0)), \end{aligned} \tag{23}$$

and relation (11) leads to

$$\hat{a}_{\mathrm{out}}(\omega_0) = R(\omega_0) \hat{a}_{\mathrm{in}}(\omega_0), \tag{24}$$

with the reflection coefficient

$$R(\omega_0) = -1 - \frac{2\gamma_{\mathrm{TL}}}{\tilde{\gamma}} \left[P_0(\omega_0) - P_1(\omega_0) \right]. \tag{25}$$

Inverse Fourier transform of Equation (24) yields the time-domain relation

$$\begin{aligned} \hat{a}_{\mathrm{out}}(t) &= \mathcal{F}^{-1} \left[R(\omega_0) \right] * \mathcal{F}^{-1} \left[\hat{a}_{\mathrm{in}}(\omega_0) \right] && (26) \\ &= R(t) \hat{a}_{\mathrm{in}}(t), && (27) \end{aligned}$$

where we have only to substitute $P_{0/1}(\omega_0)$ with $P_{0/1}(t)$ in Equation (25) for R, because $\hat{a}_{\mathrm{in}} \propto \delta(\omega - \omega_0)$, which makes the resulting convolution easy to solve. The reflection coefficient in our system can be greater than one if $P_0(t) < P_1(t)$, because in this case the incoming signal can be amplified by spontaneous or stimulated emission.

Note that all the equations (23)-(27) are also valid for the non-resonant case, provided one substitutes ω_0 in (22) with ω_s.

To obtain the rate equations for the system, we replace $\hat{\mathcal{P}}_0$, $\hat{\mathcal{P}}_1$, and $\hat{\mathcal{P}}_m$ with the corresponding occupation probabilities P_0, P_1, and P_m, which leads to

$$\begin{aligned} \dot{P}_0 = &-\gamma_0 P_0 + (\gamma_{\mathrm{TL}} + \gamma_{\mathrm{rel}}) P_1 && (28) \\ &- \sqrt{\gamma_{\mathrm{TL}}} \left(\left\langle \hat{a}_{\mathrm{in}}^\dagger \hat{\sigma} \right\rangle + \left\langle \hat{\sigma}^\dagger \hat{a}_{\mathrm{in}} \right\rangle \right) + \gamma_{\mathrm{res}} P_m && (29) \end{aligned}$$

$$\dot{P}_1 = -(\gamma_{\mathrm{TL}} + \gamma_1 + \gamma_{\mathrm{rel}}) P_1 + \sqrt{\gamma_{\mathrm{TL}}} \left(\left\langle \hat{a}_{\mathrm{in}}^\dagger \hat{\sigma} \right\rangle + \left\langle \hat{\sigma}^\dagger \hat{a}_{\mathrm{in}} \right\rangle \right) \tag{30}$$

$$\dot{P}_m = \gamma_0 P_0 + \gamma_1 P_1 - \gamma_{\mathrm{res}} P_m. \tag{31}$$

Using relation (11) and the expression for R, we end up with a system of coupled rate equations where we have eliminated $\hat{\sigma}$ and $\hat{\sigma}^\dagger$:

$$\dot{P}_0 = -(4P_{\mathrm{in}} + \gamma_0) P_0 + (4P_{\mathrm{in}} + \gamma_{\mathrm{TL}} + \gamma_{\mathrm{rel}}) P_1 + \gamma_{\mathrm{res}} P_m \tag{32}$$

$$\dot{P}_1 = 4P_{\mathrm{in}} P_0 - (4P_{\mathrm{in}} + \gamma_{\mathrm{TL}} + \gamma_1 + \gamma_{\mathrm{rel}}) P_1, \tag{33}$$

$$\dot{P}_m = \gamma_0 P_0 + \gamma_1 P_1 - \gamma_{\mathrm{res}} P_m. \tag{34}$$

Here we define the parameter P_{in} proportional to the incoming photon flux $N_{\mathrm{in}} \equiv \left\langle \hat{a}_{\mathrm{in}}^\dagger \hat{a}_{\mathrm{in}} \right\rangle$ as follows:

$$P_{\mathrm{in}} \equiv \frac{\gamma_{\mathrm{TL}}}{\tilde{\gamma}} N_{\mathrm{in}}. \tag{35}$$

The overall measurement efficiency is given in the stationary state; therefore, we set $\dot{P}_0 = \dot{P}_1 = \dot{P}_m = 0$. Doing so and using the constraint $P_0 + P_1 + P_m = 1$, we end up with an expression for stationary P_0, and P_1:

$$\begin{aligned} P_0 = &\frac{1}{1 + \frac{\gamma_0}{\gamma_{\mathrm{res}}}} \\ &- \frac{4\gamma_{\mathrm{TL}} N_{\mathrm{in}}}{\tilde{\gamma} \left(4N_{\mathrm{in}} \frac{\gamma_{\mathrm{TL}}}{\tilde{\gamma}} \left[\frac{\gamma_{\mathrm{res}} + \gamma_1}{\gamma_{\mathrm{res}} + \gamma_0} \right] + \gamma_{\mathrm{TL}} + \gamma_1 + \gamma_{\mathrm{rel}} \right) \left(1 + \frac{\gamma_0}{\gamma_{\mathrm{res}}} \right)^2} \end{aligned} \tag{36}$$

$$P_1 = \frac{4\gamma_{\mathrm{TL}} N_{\mathrm{in}}}{\tilde{\gamma} \left(4N_{\mathrm{in}} \frac{\gamma_{\mathrm{TL}}}{\tilde{\gamma}} \left[\frac{\gamma_{\mathrm{res}} + \gamma_1}{\gamma_{\mathrm{res}} + \gamma_0} \right] + \gamma_{\mathrm{TL}} + \gamma_1 + \gamma_{\mathrm{rel}} \right) \left(1 + \frac{\gamma_0}{\gamma_{\mathrm{res}}} \right)}. \tag{37}$$

To get from equations (32)-(34) to the expressions (36), (37) we had to assume that $\gamma_{\mathrm{res}} > 0$, such that the expressions for P_0 and P_1 are only valid for the case $\gamma_{\mathrm{res}} \neq 0$. The exact solution for the case $\gamma_{\mathrm{res}} = 0$ is given in Appendix B.

The dark count correction is given by the counting rate in absence of incoming photons; therefore, $\Gamma_{\mathrm{dark}} = \gamma_0 P_0(N_{\mathrm{in}} = 0)$. If we use the fact that the dead time of the counter can be expressed in terms of the reset rate as $\tau_{\mathrm{dead}} = 1/\gamma_{\mathrm{res}}$, we obtain the well known expression for the dark count correction for quantum optical counters

[28]

$$\Gamma_{\text{dark}} = \gamma_0 P_0(N_{\text{in}} = 0) = \frac{\gamma_0}{1 + \gamma_0 \tau_{\text{dead}}}. \tag{38}$$

The overall counting rate on the other hand is given by

$$\Gamma_{\text{count}} = \gamma_1 P_1(N_{\text{in}}) + \gamma_0 P_0(N_{\text{in}}). \tag{39}$$

With (38) and (39), the bright count rate, which describes the rate at which incoming photons are detected, can be written as

$$\Gamma_{\text{bright}} = \Gamma_{\text{count}} - \Gamma_{\text{dark}}. \tag{40}$$

The fidelity of a photon counter can in general be characterized by its efficiency, which is defined as the rate of detected photons Γ_{bright} over the rate of incident photons $\Gamma_{\text{incident}} = N_{\text{in}}$ [28]. For the JPM, the efficiency is given by

$$\eta = \frac{\Gamma_{\text{bright}}}{\Gamma_{\text{incident}}} \tag{41}$$

$$= \frac{1}{N_{\text{in}}} \left[\gamma_1 P_1(N_{\text{in}}) + \gamma_0 P_0(N_{\text{in}}) - \gamma_0 P_0(N_{\text{in}} = 0)\right]. \tag{42}$$

If we put the expressions for P_0 and P_1 into (42), we obtain an overall expression for the detection efficiency:

$$\eta = \frac{4\gamma_{\text{TL}}\gamma_{\text{res}} \left[\gamma_1 \left(\gamma_0 + \gamma_{\text{res}}\right) + \gamma_0 \left(\gamma_1 + \gamma_{\text{res}}\right)\right]}{(\gamma_{\text{TL}} + \gamma_1 + \gamma_{\text{rel}})(\gamma_{\text{TL}} + \gamma_1 + \gamma_0 + \gamma_{\text{rel}}) \left(\gamma_0 + \gamma_{\text{res}}\right)^2}, \tag{43}$$

where we have assumed the low excitation limit ($N_{\text{in}} \ll 1$), such that the terms proportional to N_{in} in the denominators of (36) and (37) can be ignored. The efficiency possesses a distinct maximum (see Fig. 2) that is reached when the following relation between rates is satisfied

$$\gamma_{\text{TL}}^{\text{max}} = \sqrt{(\gamma_1 + \gamma_{\text{rel}})(\gamma_1 + \gamma_{\text{rel}} + \gamma_0)}. \tag{44}$$

We refer to this expression as the matching condition. If the rates are chosen such that (44) is satisfied, we say the JPM and the transmission line are matched, to make a connection to impedance matching in microwave circuits [43]. When the JPM is matched to the transmission line, we find an efficiency

$$\eta_{\text{max}} = \frac{4(\gamma_0 + \gamma_1)}{\gamma_0 + 2\left(\gamma_1 + \gamma_{\text{rel}} + \sqrt{(\gamma_1 + \gamma_{\text{rel}})(\gamma_0 + \gamma_1 + \gamma_{\text{rel}})}\right)}, \tag{45}$$

where we assume the reset to happen faster than the measurement process $\gamma_{\text{res}} > \gamma_1$, such that the efficiency is independent of the reset rate (see Fig. 3).

If there are no dark counts and no relaxation, the efficiency is given by

$$\eta = \frac{4\gamma_{\text{TL}}\gamma_1}{(\gamma_{\text{TL}} + \gamma_1)^2}, \tag{46}$$

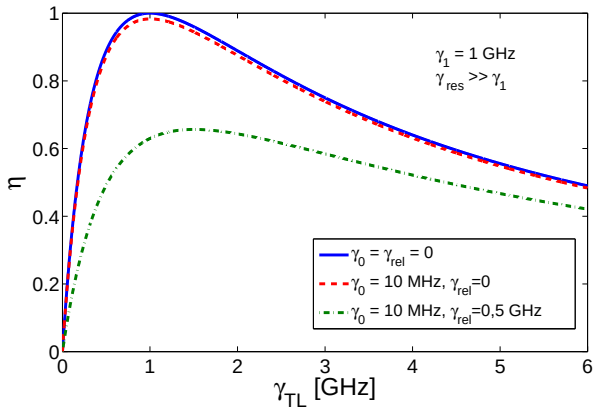

FIG. 2. Efficiency η as a function of the coupling rate γ_{TL}. The efficiency has a distinct maximum value given by equation (44) that depends on γ_0, γ_1, γ_{rel}. For $\gamma_0 = \gamma_{\text{rel}} = 0$ (blue), the matching condition simplifies to (47) and the efficiency reaches 1. An additional dark count rate γ_0 (red) leads to a small shift and reduction of the maximum value; both are barely visible for typical values of γ_0. On the other hand, the inclusion of relaxation γ_{rel} (green) reduces the maximum value significantly and furthermore leads to a visible shift of the maximum to higher values of γ_{TL}.

and the matching condition simplifies to

$$\gamma_{\text{TL}} = \gamma_1, \tag{47}$$

where the efficiency reaches 1, in case $\gamma_{\text{res}} > \gamma_1$.

This result coincides with the optimal matching condition found in Romero *et al.* [44]; however, the efficiency was limited to 1/2. The reason for this is that Romero *et al.* assumed an infinite transmission line with a JPM in the middle. Therefore, an excitation in the JPM can spontaneously emit into the other side of the transmission line at a rate γ_{TL}, allowing for transmission through the JPM. For maximum efficiency $\gamma_{\text{TL}} = \gamma_1$, both photon detection and photon transmission through the JPM will occur with equal probability, reducing the efficiency to 1/2. In this work, we assume a semi-infinite transmission line terminated by the JPM, such that the transmission process is not possible, which leads to a maximum efficiency of 1.

In our case there are four main processes that limit detector efficiency: coupling losses (reflection), energy relaxation, dark counts, and dead time. Usually one distinguishes between two separate efficiencies: the efficiency due to coupling losses η_{loss} and the intrinsic quantum efficiency of the detector η_{det}. Here, η_{loss} includes the effect of rate mismatch between the JPM and the transmission line, as described above. On the other hand, η_{det} includes the effects of dark counts, relaxation, and dead time. The overall efficiency can be written as the product of these two: $\eta = \eta_{\text{loss}} \cdot \eta_{\text{det}}$.

In the ideal case ($\gamma_0 = \gamma_{\text{rel}} = 0$ and $\gamma_{\text{res}} \ll \gamma_1$, so that $\eta_{\text{det}} = 1$), the efficiency is only limited by η_{loss}. Condition (47) then determines the coupling rate for which

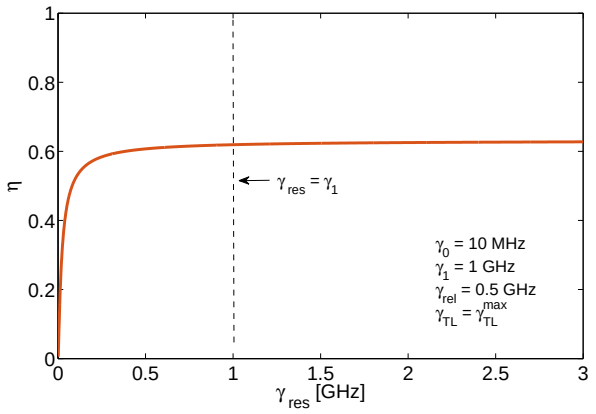

FIG. 3. Efficiency η as a function of the reset rate $\gamma_{\rm res}$. For small values of $\gamma_{\rm res}$, increasing the reset rate leads to a strong enhancement of the efficiency up to a point where the reset is roughly as fast as the decay into the measurement state ($\gamma_{\rm res} \approx \gamma_1$). From then on the efficiency stays constant with increasing $\gamma_{\rm res}$, since the reset is faster than the average measurement time.

coupling loss is zero, such that $\eta_{\rm loss} = 1$ and we reach unit efficiency (see Fig. 2). This is exactly the point where all incoming photons reach the measurement state of the counter and all the incoming power is transferred into a measured signal.

In the non-ideal case where we have dark counts and relaxation, even at the matching point (44) the efficiency is limited to a value smaller than one (since $\eta_{\rm det} < 1$), such that the optimal power matching condition (44) can only lead to an overall efficiency of $\eta_{\rm det}$ (see Fig. 2).

In Fig. 3, we see that the reset time also has a significant influence on $\eta_{\rm det}$. For $\gamma_{\rm res} < \gamma_1$, the efficiency increases rapidly with increasing $\gamma_{\rm res}$ up to the point where $\gamma_{\rm res} \approx \gamma_1$, after which the efficiency is approximately constant if we increase $\gamma_{\rm res}$. This can be explained by the fact that for a system with $\gamma_{\rm res} \approx \gamma_1$, the reset happens with the same rate as the measurement, such that increasing $\gamma_{\rm res}$ no longer has an influence on $\eta_{\rm det}$.

In many applications to detection of continuous-wave signals, it is helpful to express detector performance in terms of noise equivalent power (NEP), the effective noise power per unit bandwidth referred to the detector input. In the case of a photon counter with dark count rate γ_0 operated for an integration time τ, Poisson uncertainty in the number of dark counts is given by $\sigma_N = \sqrt{\gamma_0 \tau}$. Expressing this uncertainty as a photon flux at the input, we find

$$\sigma_P = \frac{\hbar\omega_0}{\eta\tau}\sqrt{\gamma_0\tau}. \tag{48}$$

If we choose an integration time of 0.5 s, corresponding to a detection bandwidth of 1 Hz, we obtain the standard expression for the NEP of a photon counter [28, 58]

$$\mathrm{NEP} = \frac{\hbar\omega_0}{\eta}\sqrt{2\gamma_0}; \tag{49}$$

if we put in the expression (43) for JPM efficiency, we obtain the NEP for the JPM. For the JPM parameters $\gamma_{\rm rel} = 33$ kHz [4], $\gamma_1 = 1$ GHz, $\gamma_0 = \gamma_1/100$ and $\omega_0/2\pi = 5$ GHz, we find an NEP of 2×10^{-20} W/$\sqrt{\rm Hz}$ at the matching point. This is to be compared against NEP of order 1×10^{-17} W/$\sqrt{\rm Hz}$ achieved by transition edge sensors (TES) [59] and microwave kinetic inductance detectors (MKIDs) [60] at higher frequencies in the range from 40-300 GHz, relevant for cosmic microwave background (CMB) studies. It is possible that Josephson junctions based on higher-gap materials such as NbN could be used to realize JPMs with plasma frequencies in the tens of GHz range, suitable for low-noise detection of the CMB.

IV. MEAN FIELD APPROACH

In this section, we use a mean field approach (see [61]) to simplify equations (20a)-(20e). This approach is a better approximation than the rate equation approach of the previous section, since it includes first order correlations between the transmission line and the JPM.

Before solving the equations, we take the expectation value with respect to the transmission line state, tracing out the degrees of freedom of the transmission line. Because of the normal ordering of the Hamiltonian (8), taking the expectation value of the transmission line ignores vacuum contributions to the system.

In the following, we only consider one measurement event ($\gamma_{\rm res} = 0$) and look at the pure measurement probability to define the efficiency of the counter, since this value corresponds to the efficiency in the multi-count case (for short enough reset time). Additionally, we ignore dark counts ($\gamma_0 = 0$) since we have seen in the previous section that typical dark count rates do not change the results significantly. For simplicity we also assume that we do not have any relaxation ($\gamma_{\rm rel} = 0$).

A. Continuous Drive

We assume that we have a continuous, coherent drive at frequency ω_0 and photon amplitude α, such that the initial state reads

$$|\Phi(t=0)\rangle = |0\rangle_{\rm JPM} \otimes |\alpha_{\omega_0}\rangle_{\rm TL} = |0, \alpha_{\omega_0}\rangle\,, \tag{50}$$

where the JPM is arranged in the ground state before measurement and the transmission line is in a coherent state of amplitude α and frequency ω_0. We can take the expectation value in the system of equations (20a)-(20e) with respect to state (50) (note that the time dependence is included in the operators, such that $|\Phi\rangle$ stays

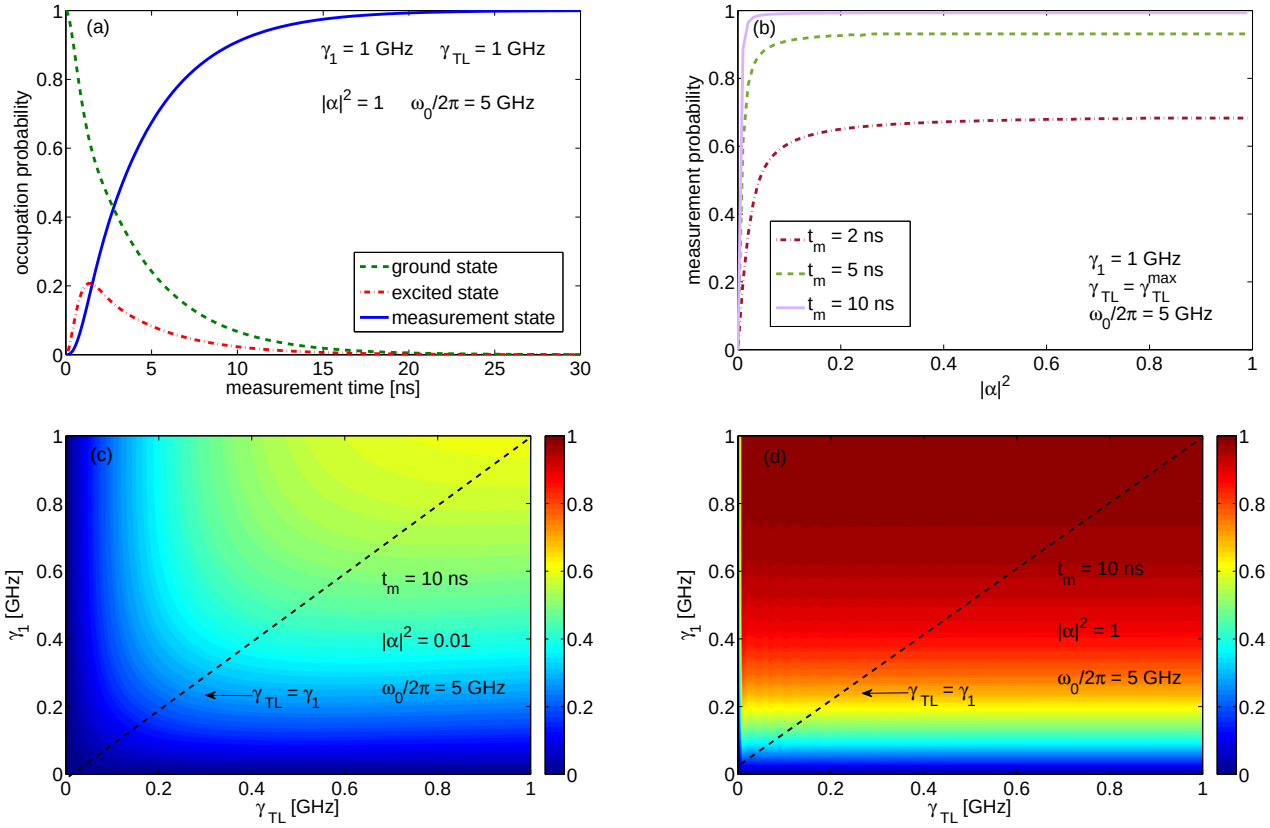

FIG. 4. (a) Occupation probabilities as a function of the measurement time t_m. (b) Measurement probability as a function of $|\alpha|^2$ for a measurement time of $t_m = 10$ ns and matched rates $\gamma_{\rm TL} = \gamma_{\rm TL}^{\rm max}$ (before steady state is reached). One sees a saturation at around 0.2 photons, such that increasing $|\alpha|^2$ further does not increase the measurement probability. (c),(d) Detection probability versus the rates $\gamma_{\rm TL}$ and γ_1 after $t_m = 10$ ns (before stationary state is reached) for two different values of $|\alpha|^2$. (c) For small values of $|\alpha|^2$, the optimal measurement regime coincides with the matching condition (47) found in Section II. (d) For high values of $|\alpha|^2$, we see a plateau behavior, such that the measurement probability is independent of $\gamma_{\rm TL}$.

constant). To trace out the transmission line degrees of freedom, we apply $\hat{a}_{\rm in}$ to the right and $\hat{a}_{\rm in}^\dagger$ to the left, which gives

$$\hat{a}_{\rm in}\,|0,\alpha_{\omega_0}\rangle = -\frac{i}{\sqrt{2\pi}}\alpha\sqrt{\omega_0}\exp[-i\omega_0 t]\,|0,\alpha_{\omega_0}\rangle\,. \qquad (51)$$

In addition we apply the transformation $\hat{\sigma} \longmapsto \exp[-i\omega_0 t]\hat{\sigma}$ and $\hat{\sigma}^\dagger \longmapsto \exp[i\omega_0 t]\hat{\sigma}^\dagger$ in order to make the equations time independent. After these steps, we finally end up with equations of motion for the expectation values of the JPM operators:

$$\left\langle\dot{\hat{\sigma}}\right\rangle = -\frac{\tilde{\gamma}}{2}\left\langle\hat{\sigma}\right\rangle - \mathrm{i}\frac{\omega_{\rm R}}{2}\left(\left\langle\hat{\mathcal{P}}_0\right\rangle - \left\langle\hat{\mathcal{P}}_1\right\rangle\right) \qquad (52a)$$

$$\left\langle\dot{\hat{\sigma}}^\dagger\right\rangle = -\frac{\tilde{\gamma}}{2}\left\langle\hat{\sigma}^\dagger\right\rangle + \mathrm{i}\frac{\omega_{\rm R}}{2}\left(\left\langle\hat{\mathcal{P}}_0\right\rangle - \left\langle\hat{\mathcal{P}}_1\right\rangle\right) \qquad (52b)$$

$$\left\langle\dot{\hat{\mathcal{P}}}_0\right\rangle = \gamma_{\rm TL}\left\langle\hat{\mathcal{P}}_1\right\rangle - \mathrm{i}\frac{\omega_{\rm R}}{2}\left(\left\langle\hat{\sigma}\right\rangle - \left\langle\hat{\sigma}^\dagger\right\rangle\right) \qquad (52c)$$

$$\left\langle\dot{\hat{\mathcal{P}}}_1\right\rangle = -\tilde{\gamma}\left\langle\hat{\mathcal{P}}_1\right\rangle + \mathrm{i}\frac{\omega_{\rm R}}{2}\left(\left\langle\hat{\sigma}\right\rangle - \left\langle\hat{\sigma}^\dagger\right\rangle\right) \qquad (52d)$$

$$\left\langle\dot{\hat{\mathcal{P}}}_m\right\rangle = \gamma_1\left\langle\hat{\mathcal{P}}_1\right\rangle, \qquad (52e)$$

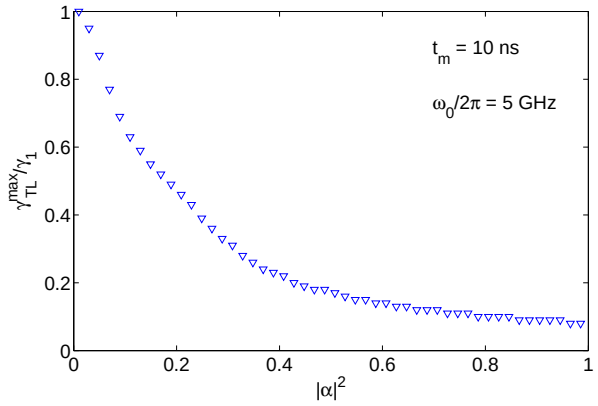

FIG. 5. Dependence of $\gamma_{\rm TL}^{\rm max}/\gamma_1$ on $|\alpha|^2$ for the continuous drive case. For small values of $|\alpha|^2$, the optimal regime is the matching condition (47) found in Section III. For higher values of $|\alpha|^2$ the optimal measurement regime shifts to smaller ratios $\gamma_{\rm TL}^{\rm max}/\gamma_1$, since the Rabi frequency is proportional to $\sqrt{\gamma_{\rm TL}|\alpha|^2}$.

where $\omega_R \equiv \sqrt{2|\alpha|^2\gamma_{\rm TL}\omega_0/\pi}$ denotes the Rabi frequency, and where we have used the relation $\langle\hat{\sigma}_z\rangle = \left\langle\hat{\mathcal{P}}_0\right\rangle - \left\langle\hat{\mathcal{P}}_1\right\rangle$ to eliminate $\langle\hat{\sigma}_z\rangle$. This system of equations can be solved numerically (see Fig. 4).

We are mostly interested in the probability of detection $\left\langle\hat{\mathcal{P}}_m\right\rangle$. For every choice of parameters, the measurement probability reaches one after some time since we assume a continuous drive (see Fig. 4(a)), so that energy transfer to the JPM continues for as long as needed to tunnel to the measurement state. The switching time depends on the choice of parameters, and we see that for small values of $|\alpha|^2$, the condition that minimizes this time is exactly the matching condition we found in Section II (see Fig.4(c) and Fig. 5).

For higher values of $|\alpha|^2$, the matching condition shifts to smaller values of $\gamma_{\rm TL}$ (see Fig. 5). This can be explained by the fact that the transition time to the $|1\rangle$ state in the JPM is determined by the Rabi frequency ω_R, which is proportional to the product of $\gamma_{\rm TL}$ and $|\alpha|^2$. Therefore, higher values of $|\alpha|^2$ lead to smaller values of $\gamma_{\rm TL}$ in the matching condition, since ω_R has to be in the range of γ_1. If we match the rates and look at the $|\alpha|^2$ dependence of the measurement probability, we see a saturation point at a fixed value of $|\alpha|^2$ (see Fig. 4(b)). This means that adding more photons does not increase the measurement probability, since the JPM can only measure one photon (see Fig. 4(b)). The measurement probability is one at this saturation point if the measurement time is longer than the required time for a tunneling process, and smaller than one otherwise (see Fig. 4(b)). Moreover, we find that for high values of $|\alpha|^2$ there is a large region where the measurement probability is independent of $\gamma_{\rm TL}$ and only varies with γ_1 (see Fig. 4(d)).

In Appendix B, we solve the time evolution of the rate equations of Section II analytically to compare them to the results reached in this Section for the continuous drive case. The comparison is shown in Fig. 6. We see that the results of both approaches are very similar for both the classical and the quantum regimes. In Appendix C, we additionally provide an analytical solution for the continuous mean field approach using the Laplace transformation.

B. Pulses

For applications to qubit measurement [38] we wish to perform threshold detection on an input pulse of n photons. Therefore, we want to extend the above solutions to the more general case of an arbitrary input waveform. To do so, we add a form factor $f(\omega)$ that describes the pulse into the expression for $\hat{a}_{t_0}(\omega)$

$$\begin{aligned}\hat{a}_{\rm pulse}(\omega) &= f(-\omega)\hat{a}_{t_0}(\omega)\\ \hat{a}^\dagger_{\rm pulse}(\omega) &= f(\omega)\hat{a}^\dagger_{t_0}(\omega),\end{aligned} \tag{53}$$

where we assume the form factor to be real. We incorporate this form factor into the system of equations and follow the same procedure as in the previous Section.

By using the Fourier relation $\int_{-\infty}^{\infty}\mathrm{d}\omega f(\pm\omega)\exp\left(\mp\mathrm{i}(\omega-\omega_0)\mathrm{t}\right) = f(t)$, we can bring the resulting system of equations to the following form:

$$\left\langle\dot{\hat{\sigma}}\right\rangle = -\frac{\tilde{\gamma}}{2}\left\langle\hat{\sigma}\right\rangle - i\frac{\omega_R}{2}f(t)\left(\left\langle\hat{\mathcal{P}}_0\right\rangle - \left\langle\hat{\mathcal{P}}_1\right\rangle\right) \tag{54a}$$

$$\left\langle\dot{\hat{\sigma}}^\dagger\right\rangle = -\frac{\tilde{\gamma}}{2}\left\langle\hat{\sigma}^\dagger\right\rangle + i\frac{\omega_R}{2}f(t)\left(\left\langle\hat{\mathcal{P}}_0\right\rangle - \left\langle\hat{\mathcal{P}}_1\right\rangle\right) \tag{54b}$$

$$\left\langle\dot{\hat{\mathcal{P}}}_0\right\rangle = \gamma_{\rm TL}\left\langle\hat{\mathcal{P}}_1\right\rangle - i\frac{\omega_R}{2}f(t)\left(\left\langle\hat{\sigma}\right\rangle - \left\langle\hat{\sigma}^\dagger\right\rangle\right) \tag{54c}$$

$$\left\langle\dot{\hat{\mathcal{P}}}_1\right\rangle = -\tilde{\gamma}\left\langle\hat{\mathcal{P}}_1\right\rangle + i\frac{\omega_R}{2}f(t)\left(\left\langle\hat{\sigma}\right\rangle - \left\langle\hat{\sigma}^\dagger\right\rangle\right) \tag{54d}$$

$$\left\langle\dot{\hat{\mathcal{P}}}_m\right\rangle = \gamma_1\left\langle\hat{\mathcal{P}}_1\right\rangle, \tag{54e}$$

where $\omega_R \equiv \sqrt{2|\alpha|^2\gamma_{\rm TL}\omega_s/\pi}$. This system of equations is similar that in the previous section, apart from an additional factor $f(t)$ that specifies the pulse shape. Using these equations, we can solve for the time evolution of the state occupations for an arbitrary pulse shape.

Here, we study two different shapes, an exponential damped pulse and a Gaussian pulse. The first pulse shape is especially relevant for qubit measurement, since it describes the shape of a pulse created from a spontaneous emission source [62]. This pulse is described by the form factor

$$f(t) = \exp\left(-\kappa t\right), \tag{55}$$

with signal frequency ω_s of the pulse and duration $\tau_e = 2\pi/\kappa$. We assume the signal frequency to be equal to the JPM transition frequency, $\omega_s = \omega_0$.

Next, we study the most natural choice for a few-photon wave packet, namely the Gaussian pulse

$$\begin{aligned}f(\omega) &= \frac{1}{(2\pi\sigma^2\omega_s^2)^{\frac{1}{4}}}\exp\left(-\frac{(\omega-\omega_s)^2}{4\sigma^2}\right)\\ f(t) &= \left(\frac{8\pi\sigma^2}{\omega_s^2}\right)^{\frac{1}{4}}\exp\left(-\sigma^2t^2\right),\end{aligned} \tag{56}$$

with duration $\tau_G = 2\pi/\sigma$. We assume the signal frequency ω_s to coincide with the transition frequency of the JPM ($\omega_s = \omega_0$). The results are similar to the results for the exponentially damped pulse, except that σ plays the role of κ in this case (see Fig. 7).

For small photon numbers $|\alpha|^2$, we observe the matching condition (47) we found in Section II. Increasing $|\alpha|^2$ shifts the maximum regime to higher values of γ_1 and smaller values of $\gamma_{\rm TL}$, for the same reason as in the continuous drive case. The behavior of $\gamma_{\rm TL}^{\rm max}/\gamma_1$ for a Gaussian pulse is shown in Fig. 7(b) for two different values of σ. We see that the ratio starts at one and then immediately drops to smaller values before asymptotically tending to zero in the semi-classical regime. The movement of the optimal measurement region is also shown in Fig. 7(e-f).

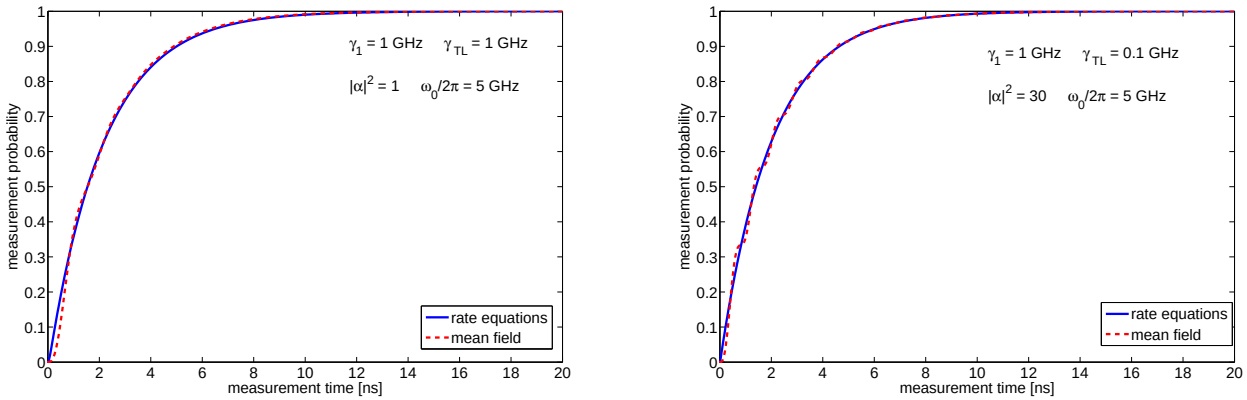

FIG. 6. Comparison of rate equation (blue) and mean field (red) approaches, in the quantum (left) and classical regimes (right). The two approaches give similar results apart from the absence of Rabi oscillations in the rate equation approach, where the JPM is treated classically.

On the other hand, the maximum of the measurement probability for fixed values of $|\alpha|^2$ depends on the parameters κ and σ for the exponentially damped and Gaussian pulse, respectively (see Fig. 7(c),(d)). In the exponentially damped case, the measurement probability in the steady state is unity for very small κ (long pulses); hence it coincides with the continuous drive result in this regime. If we go over to shorter pulses, κ plays an important role in the overall measurement probability. For the Gaussian pulse, we do not see a constant plateau where $P_m = 1$ for very small values of σ; rather, P_m only reaches unity for $\sigma = 0$, which corresponds to a continuous drive.

For the exponentially damped pulse, it is also possible to obtain analytical results using the Laplace transformation. We find the following expression for the measurement probability in the stationary state

$$\left\langle \hat{\mathcal{P}}_m(t) \right\rangle = \frac{\omega_R^2}{4\kappa\left(\kappa+\frac{\tilde{\gamma}}{2}\right)\left(1+\frac{\gamma_{\mathrm{TL}}}{\gamma_1}\right)} - \sum_{l=0}^{\infty} \frac{\omega_R^2}{2} \frac{1+4\frac{\kappa}{\gamma_1}}{\left(\kappa+\frac{\tilde{\gamma}}{2}\right)\left(1+\frac{\gamma_{\mathrm{TL}}}{\gamma_1}\right)} \frac{\left\langle \hat{\mathcal{P}}_m(0)^{(l)} \right\rangle}{(2\kappa)^{-(l+1)}}. \tag{57}$$

For given initial conditions of the system and starting with the set of equations (54a)-(54e), one can calculate $\left\langle \hat{\mathcal{P}}_m(0)^{(l)} \right\rangle$ to arbitrary order (for more details see Appendix D).

V. CONCLUSION

In conclusion, we have derived a general set of equations that describe a two-level photon counter strongly coupled to a transmission line. We have shown that one can reach high-efficiency photon detection of a traveling microwave state using appropriate matching of system parameters. The conditions vary for different input states; in general, for low input power the coupling rate between the counter and the transmission line should be equal to the measurement rate. At higher power, the matching condition shifts, such that the coupling rate should be smaller than the measurement rate.

The approach described here can be applied to arbitrary input pulses and thus modified to fit the particular radiation source of any experiment. As a result, this work presents a guide to tune parameters to reach the optimal measurement efficiency for a range of experimental situations. Moreover, the presented method can be extended to any lossy two-level system coupled to a semi-infinite resonator.

ACKNOWLEDGEMENTS

We thank B. Taketani, Guilhem Ribeill, Ivan Pechenezhskiy and Ted Thorbeck for fruitful discussions. Supported by the Army Research Office under contract W911NF-14-1-0080. LCGG and FKW also acknowledge support from the European Union through ScaleQIT and LCGG from NSERC through an NSERC PGS-D.

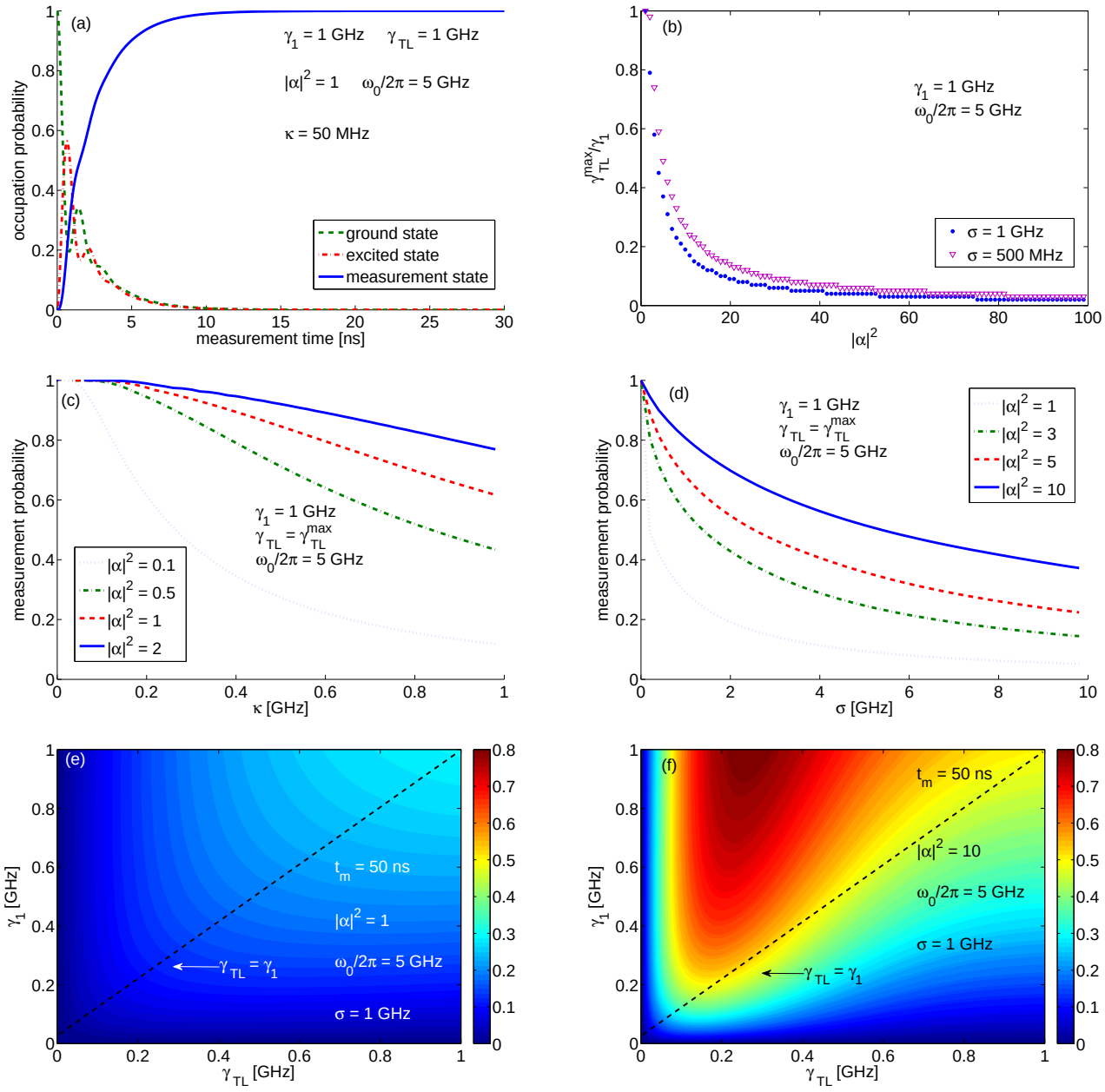

FIG. 7. Results for shaped pulse inputs. (a) Time evolution of the state occupation probabilities for an exponentially damped pulse with mean photon number $|\alpha|^2 = 1$. (b) Dependence of the optimal choice of rates $\gamma_{\rm TL}^{\rm max}/\gamma_1$ on $|\alpha|^2$ for a Gaussian pulse. (c),(d) Dependence of the optimal detection probability depending on κ and σ for exponentially damped and Gaussian pulses, respectively. (e), (f) Shift of the optimal measurement region for different values of $|\alpha|^2$ in the Gaussian case.

Appendix A: Hamiltonian of the system

From the circuit diagram Fig. 1 we can derive the Lagrangian of the system:

$$\begin{aligned}\mathcal{L} &= \mathcal{L}_{\rm TL} + E_J\cos(\varphi_J) + (I_b + \Delta I)\left(\frac{\Phi_0}{2\pi}\right)\varphi_J \\ &\quad + \frac{1}{2}C_J\left(\frac{\Phi_0}{2\pi}\right)^2\dot{\varphi}_J^2 \\ &= \mathcal{L}_{\rm TL} + \mathcal{L}_{\rm JPM} + \Delta I\left(\frac{\Phi_0}{2\pi}\right)\varphi_J + \frac{1}{2}C_J\left(\frac{\Phi_0}{2\pi}\right)^2\dot{\varphi}_J^2,\end{aligned} \tag{A1}$$

where $\mathcal{L}_{\rm TL}$ is the bare transmission line Lagrangian (sum of harmonic oscillators), φ_J the phase of the JPM, I_b the bias current, E_J the Josephson energy, C_J the junction capacitance, Φ_0 the flux quantum, and ΔI the additional current coming from the transmission line. Here, $\mathcal{L}_{\rm JPM} \equiv E_J\cos(\varphi_J) + I_b\frac{\Phi_0}{2\pi}\varphi_J$ is the Lagrangian of the JPM. The last term leads to an interaction between the JPM and the transmission line. Using the Legendre transformation, we obtain the Hamiltonian of the sys-

tem:

$$\mathcal{H} = \mathcal{H}_{\mathrm{TL}} + \mathcal{H}_{\mathrm{SYS}} + \Delta I \frac{\Phi_0}{2\pi}\varphi_J, \tag{A2}$$

where $\mathcal{H}_{\mathrm{TL}}$ is the Hamiltonian describing the transmission line and $\mathcal{H}_{\mathrm{JPM}}$ is the Hamiltonian of the JPM.

We want to take a closer look at the interaction term. If we use the normal procedure of quantizing the transmission line and the JPM, we get the following expression for the current [50] and phase operators [49]:

$$\Delta\hat{I} = \sqrt{\frac{\hbar\omega_s}{4\pi Z_0}}\int_0^\infty \mathrm{d}\omega\left(\hat{a}^\dagger(\omega) + \hat{a}(\omega)\right) \tag{A3}$$

$$\hat{\varphi}_J = \frac{i}{\sqrt{2}}\left(\frac{2E_C}{E_J}\right)^{\frac{1}{4}}\left(\hat{\sigma}^\dagger - \hat{\sigma}\right), \tag{A4}$$

where $\hat{a}$,$\hat{a}^\dagger$ and $\hat{\sigma}$,$\hat{\sigma}^\dagger$ are the raising and lowering operators of the cavity field and the JPM states, respectively. Equations (A2)-(A4) assuming an rotating-wave approximation lead to the following expression for the interaction part of the Hamiltonian (infinite number of input modes):

$$\hat{H}_{\mathrm{INT}} = i\hbar g\int_{-\infty}^{\infty}\mathrm{d}\omega(\hat{a}^\dagger(\omega)\hat{\sigma} - \hat{\sigma}^\dagger(\omega)\hat{a}), \tag{A5}$$

with $g \equiv (\omega_s Z_J/8\pi Z_0)^{1/2}$, where Z_J is the junction impedance.

Appendix B: Time dynamics of the rate equations

Here we want to study the time evolution of the system of rate equations (32)-(34) for a single measurement event ($\gamma_{\mathrm{res}} = 0$). Using an algebraic computer software package, we obtain the following solution for the occupation probability of the excited state for initial conditions $P_0 = 1$ and $P_1 = 0$:

$$P_1(t) = \beta\sinh\left(\Gamma t\right), \tag{B1}$$

with the constant

$$\beta = \frac{4\gamma_{\mathrm{TL}}\tilde{\omega}}{\sqrt{\left(\gamma_{\mathrm{TL}}+\gamma_1\right)^4 + 16\gamma_{\mathrm{TL}}^2\left(\gamma_{\mathrm{TL}}+\gamma_1\right)\tilde{\omega} + 64\gamma_{\mathrm{TL}}^2\gamma_1^2}} \tag{B2}$$

and the rate

$$\Gamma = \frac{\sqrt{16\gamma_{\mathrm{TL}}^2\omega_0\tilde{\gamma} + 64\gamma_{\mathrm{TL}}^2\tilde{\omega}^2 + \tilde{\gamma}^4} + \tilde{\gamma}^2 + 8\gamma_{\mathrm{TL}}\tilde{\omega}}{2\tilde{\gamma}}, \tag{B3}$$

with $\tilde{\omega} \equiv |\alpha|^2\omega_0/2\pi$. Integration of (B1) from $t' = 0$ to $t' = t$ and multiplication with γ_1, together with the boundary condition $P_m(0) = 0$, lead to an expression for the measurement probability:

$$P_m(t) = \frac{\beta\gamma_1}{\Gamma}\left[\cosh\left(\Gamma t\right) - 1\right]. \tag{B4}$$

In Section III we use expression (B4) to compare the rate equation approach with the mean field approach.

Appendix C: Analytical solution for the continuous mean field case

Here we give an analytical solution of the system of equations derived in Sec. IV A. First we use the Laplace transformation to rewrite the system:

$$s\left\langle\hat{\sigma}(s)\right\rangle = -\frac{\tilde{\gamma}}{2}\left\langle\hat{\sigma}(s)\right\rangle - \mathrm{i}\frac{\omega_{\mathrm{R}}}{2}\left(\left\langle\hat{\mathcal{P}}_0(\mathrm{s})\right\rangle - \left\langle\hat{\mathcal{P}}_1(\mathrm{s})\right\rangle\right) \tag{C1a}$$

$$s\left\langle\hat{\sigma}^\dagger(s)\right\rangle = -\frac{\tilde{\gamma}}{2}\left\langle\hat{\sigma}^\dagger(s)\right\rangle + \mathrm{i}\frac{\omega_{\mathrm{R}}}{2}\left(\left\langle\hat{\mathcal{P}}_0(\mathrm{s})\right\rangle - \left\langle\hat{\mathcal{P}}_1(\mathrm{s})\right\rangle\right) \tag{C1b}$$

$$s\left\langle\hat{\mathcal{P}}_0(s)\right\rangle = \gamma_{\mathrm{TL}}\left\langle\hat{\mathcal{P}}_1(s)\right\rangle - \mathrm{i}\frac{\omega_{\mathrm{R}}}{2}\left(\left\langle\hat{\sigma}(\mathrm{s})\right\rangle - \left\langle\hat{\sigma}^\dagger(\mathrm{s})\right\rangle\right) + 1 \tag{C1c}$$

$$s\left\langle\hat{\mathcal{P}}_1(s)\right\rangle = -\tilde{\gamma}\left\langle\hat{\mathcal{P}}_1(s)\right\rangle + \mathrm{i}\frac{\omega_{\mathrm{R}}}{2}\left(\left\langle\hat{\sigma}(\mathrm{s})\right\rangle - \left\langle\hat{\sigma}^\dagger(\mathrm{s})\right\rangle\right) \tag{C1d}$$

$$s\left\langle\hat{\mathcal{P}}_m(s)\right\rangle = \gamma_1\left\langle\hat{\mathcal{P}}_1(s)\right\rangle. \tag{C1e}$$

The first two equations give the expressions

$$\left\langle\hat{\sigma}(s)\right\rangle = -\mathrm{i}\frac{\frac{\omega_{\mathrm{R}}}{2}}{\mathrm{s}+\frac{\tilde{\gamma}}{2}}\left(\left\langle\hat{\mathcal{P}}_0(\mathrm{s})\right\rangle - \left\langle\hat{\mathcal{P}}_1(\mathrm{s})\right\rangle\right) \tag{C2}$$

$$\left\langle\hat{\sigma}^\dagger(s)\right\rangle = \mathrm{i}\frac{\frac{\omega_{\mathrm{R}}}{2}}{\mathrm{s}+\frac{\tilde{\gamma}}{2}}\left(\left\langle\hat{\mathcal{P}}_0(\mathrm{s})\right\rangle - \left\langle\hat{\mathcal{P}}_1(\mathrm{s})\right\rangle\right), \tag{C3}$$

which can be put into the equation for $\left\langle\hat{\mathcal{P}}_1(s)\right\rangle$:

$$s\left\langle\hat{\mathcal{P}}_1(s)\right\rangle = -\tilde{\gamma} + \frac{\frac{\omega_R}{2}}{s+\frac{\tilde{\gamma}}{2}}\left(\left\langle\hat{\mathcal{P}}_0(s)\right\rangle - \left\langle\hat{\mathcal{P}}_1(s)\right\rangle\right). \tag{C4}$$

Using the conservation of probabilities in Laplace space

$$\left\langle\hat{\mathcal{P}}_0(s)\right\rangle + \left\langle\hat{\mathcal{P}}_1(s)\right\rangle + \left\langle\hat{\mathcal{P}}_m(s)\right\rangle = \frac{1}{s}, \tag{C5}$$

we can eliminate $\left\langle\hat{\mathcal{P}}_0(s)\right\rangle$ in (C4):

$$s\left\langle\hat{\mathcal{P}}_1(s)\right\rangle = -\tilde{\gamma} + \frac{\frac{\omega_R}{2}}{s+\frac{\tilde{\gamma}}{2}}\left(\frac{1}{s} - 2\left\langle\hat{\mathcal{P}}_1\right\rangle(s) - \left\langle\hat{\mathcal{P}}_m(s)\right\rangle\right). \tag{C6}$$

Additionally, we can eliminate $\left\langle\hat{\mathcal{P}}_1(s)\right\rangle$ in (C6) with the equation for $\left\langle\hat{\mathcal{P}}_m(s)\right\rangle$ (C1e)

$$\left\langle\hat{\mathcal{P}}_m(s)\right\rangle = \frac{\frac{\omega_R^2}{2}}{s\left(s+\frac{\tilde{\gamma}}{2}\right)\left[\frac{s^2}{\gamma_1} + \frac{\tilde{\gamma}s}{\gamma_1} + \frac{\frac{\omega_R^2}{2}}{s+\frac{\tilde{\gamma}}{2}}\left(\frac{2s}{\gamma_1}+1\right)\right]}. \tag{C7}$$

To show that the numerical results of Section III give the right stationary solution, we can calculate $\lim_{t\to\infty}\left\langle\hat{\mathcal{P}}_m(t)\right\rangle$

from (C7) using the relation between limits in Laplace space and real space

$$\lim_{t\to\infty} g(t) = \lim_{s\to 0} s\mathcal{L}\left[g(t)\right]. \tag{C8}$$

We find

$$\lim_{t\to\infty}\left\langle\hat{\mathcal{P}}_m(t)\right\rangle = \lim_{s\to 0} s\left\langle\hat{\mathcal{P}}_m(s)\right\rangle = 1. \tag{C9}$$

Therefore the measurement probability in the stationary state is always one, as we have seen in the numerical results.

We next transform (C7) back to real space in order to get an analytical solution for the time evolution of the measurement probability. This back transformation can be done as in Section IV using the residue theorem. The singularities of (C7) are

$$\begin{aligned}
s_1 &= 0\\
s_2 &= -\frac{\tilde{\gamma}}{2} + \frac{\tilde{\gamma}^2-\omega_R^2}{2\left[54(\tilde{\gamma}-\gamma_1)\omega_R^2 + 3\sqrt{36\omega_R^2\tilde{\gamma}^4 + 36(\tilde{\gamma}-3\gamma_1)(5\tilde{\gamma}-3\gamma_1)\omega_R^4 + 194\omega_R^6}\right]^{\frac{1}{3}}}\\
&\quad + \frac{\left(\frac{27\tilde{\gamma}\omega_R^2}{2} - \frac{27\gamma_1\omega_R^2}{2} + \sqrt{\frac{729}{4}(\gamma_1-\tilde{\gamma})^2\omega_R^4 + 4\left(3\omega_R^2 - \frac{3\tilde{\gamma}^2}{4}\right)^3}\right)^{\frac{1}{3}}}{3\cdot 2^{\frac{2}{3}}}\\
s_3 &= -\frac{\tilde{\gamma}}{2} + \frac{\left(1+\mathrm{i}\sqrt{3}\right)\left(3\omega_R^2 + \frac{3\tilde{\gamma}^3}{4}\right)}{3\cdot 2^{\frac{2}{3}}\left(-\frac{27\gamma_1\omega_R^2}{2} + \frac{27\tilde{\gamma}\omega_R^2}{2} + \sqrt{4\left(3\omega_R^2 - \frac{3\tilde{\gamma}^2}{4}\right)^3 + \left(-\frac{27\gamma_1\omega_R^2}{2} + \frac{27\tilde{\gamma}\omega_R^2}{2}\right)^2}\right)^{\frac{1}{3}}}\\
&\quad - \frac{\left(1-\mathrm{i}\sqrt{3}\right)\left(-\frac{27\gamma_1\omega_R^2}{2} + \frac{27\tilde{\gamma}\omega_R^2}{2} + \sqrt{4\left(3\omega_R^2 - \frac{3\tilde{\gamma}^2}{4}\right)^3 + \left(-\frac{27\gamma_1\omega_R^2}{2} + \frac{27\tilde{\gamma}\omega_R^2}{2}\right)^2}\right)^{\frac{1}{3}}}{6\cdot 2^{\frac{1}{3}}}\\
s_4 &= s_3^*,
\end{aligned}$$

and the back transformation of (C7) is given by

$$\left\langle\hat{\mathcal{P}}_m(t)\right\rangle = \frac{\omega_R^2}{2}\sum_{\substack{i=1\\ i\neq j\neq k}}^{3}\frac{\exp\left(-s_i t\right)}{\alpha_i\left(\alpha_i-\alpha_j\right)\left(\alpha_i-\alpha_k,\right)}, \tag{C10}$$

where α_i are the corresponding residues. Due to the first order of the singularities (all other cases are trivial), the residues are given by

$$Res\left(s_i, \left\langle\hat{\mathcal{P}}_m(s)\right\rangle\right) = \lim_{s\to s_i}\left\langle\hat{\mathcal{P}}_m(s)\right\rangle(s-s_i). \tag{C11}$$

Appendix D: Analytical solution for the exponentially damped pulse

In this appendix, we calculate an analytical solution for the exponentially damped pulse. We start with the Laplace transformation of the system of equations

$$s\left\langle\hat{\sigma}(s)\right\rangle = -\frac{\tilde{\gamma}}{2}\left\langle\hat{\sigma}(s)\right\rangle - \mathrm{i}\frac{\omega_\mathrm{R}}{2}\left(\left\langle\hat{\mathcal{P}}_0(\mathrm{s}+\kappa)\right\rangle - \left\langle\hat{\mathcal{P}}_1(\mathrm{s}+\kappa)\right\rangle\right) \tag{D1a}$$

$$s\left\langle\hat{\sigma}^\dagger(s)\right\rangle = -\frac{\tilde{\gamma}}{2}\left\langle\hat{\sigma}^\dagger(s)\right\rangle + \mathrm{i}\frac{\omega_\mathrm{R}}{2}\left(\left\langle\hat{\mathcal{P}}_0(\mathrm{s}+\kappa)\right\rangle - \left\langle\hat{\mathcal{P}}_1(\mathrm{s}+\kappa)\right\rangle\right) \tag{D1b}$$

$$s\left\langle\hat{\mathcal{P}}_0(s)\right\rangle = \gamma_\mathrm{TL}\left\langle\hat{\mathcal{P}}_1(s)\right\rangle - \mathrm{i}\frac{\omega_\mathrm{R}}{2}\left(\left\langle\hat{\sigma}(\mathrm{s}+\kappa)\right\rangle - \left\langle\hat{\sigma}^\dagger(\mathrm{s}+\kappa)\right\rangle\right) + 1 \tag{D1c}$$

$$s\left\langle\hat{\mathcal{P}}_1(s)\right\rangle = -\tilde{\gamma}\left\langle\hat{\mathcal{P}}_1(s)\right\rangle + \mathrm{i}\frac{\omega_\mathrm{R}}{2}\left(\left\langle\hat{\sigma}(\mathrm{s}+\kappa)\right\rangle - \left\langle\hat{\sigma}^\dagger(\mathrm{s}+\kappa)\right\rangle\right) \tag{D1d}$$

$$s\left\langle\hat{\mathcal{P}}_m(s)\right\rangle = \gamma_1\left\langle\hat{\mathcal{P}}_1(s)\right\rangle, \tag{D1e}$$

where we have used the relation

$$\mathcal{L}\left[g(t)\exp(-\kappa t)\right] = g(s+\kappa), \tag{D2}$$

which holds for an arbitrary function $g(t)$ whose Laplace transformation exists.

To simplify the equations we have to calculate $\langle\hat{\sigma}(s+\kappa)\rangle$ and $\langle\hat{\sigma}^\dagger(s+\kappa)\rangle$, which can be done by multiplying (D1a) and (D1b) with $\exp(-\kappa t)$:

$$\langle\hat{\sigma}(s+\kappa)\rangle = \frac{-\mathrm{i}\frac{\omega_\mathrm{R}^2}{2}}{s+\kappa+\frac{\tilde{\gamma}}{2}}\left(\left\langle\hat{\mathcal{P}}_0(s+2\kappa)\right\rangle - \left\langle\hat{\mathcal{P}}_1(s+2\kappa)\right\rangle\right) \tag{D3}$$

$$\langle\hat{\sigma}^\dagger(s+\kappa)\rangle = \frac{\mathrm{i}\frac{\omega_\mathrm{R}^2}{2}}{s+\kappa+\frac{\tilde{\gamma}}{2}}\left(\left\langle\hat{\mathcal{P}}_0(s+2\kappa)\right\rangle - \left\langle\hat{\mathcal{P}}_1(s+2\kappa)\right\rangle\right). \tag{D4}$$

Putting (D3) and (D4) into (D1c) leads to

$$\begin{aligned} s\left\langle\hat{\mathcal{P}}_0(s)\right\rangle &= \gamma_\mathrm{TL}\left\langle\hat{\mathcal{P}}_1(s)\right\rangle + 1 \\ &\quad - \frac{\frac{\omega_R^2}{2}}{s+\kappa+\frac{\tilde{\gamma}}{2}}\left(\left\langle\hat{\mathcal{P}}_0(s+2\kappa)\right\rangle - \left\langle\hat{\mathcal{P}}_1(s+2\kappa)\right\rangle\right). \end{aligned} \tag{D5}$$

To eliminate $\left\langle\hat{\mathcal{P}}_0(s)\right\rangle$ in this expression, we can use the conservation of probabilities in Laplace space

$$\left\langle\hat{\mathcal{P}}_0(s)\right\rangle = \frac{1}{s} - \left\langle\hat{\mathcal{P}}_1(s)\right\rangle - \left\langle\hat{\mathcal{P}}_m(s)\right\rangle \tag{D6}$$

$$\left\langle\hat{\mathcal{P}}_0(s+2\kappa)\right\rangle = \frac{1}{s+2\kappa} - \left\langle\hat{\mathcal{P}}_1(s+2\kappa)\right\rangle - \left\langle\hat{\mathcal{P}}_m(s+2\kappa)\right\rangle, \tag{D7}$$

which gives

$$\begin{aligned} s\left(\frac{1}{s} - \left\langle\hat{\mathcal{P}}_1(s)\right\rangle - \left\langle\hat{\mathcal{P}}_m(s)\right\rangle\right) - 1 &= \gamma_\mathrm{TL}\left\langle\hat{\mathcal{P}}_1(s)\right\rangle \\ -\frac{\frac{\omega_R^2}{2}}{s+\kappa+\frac{\tilde{\gamma}}{2}}\left[\frac{1}{s+2\kappa} - 2\left\langle\hat{\mathcal{P}}_1(s)\right\rangle - \left\langle\hat{\mathcal{P}}_m(s)\right\rangle\right]. \end{aligned} \tag{D8}$$

Additionally, we can use (D1e) to eliminate $\left\langle\hat{\mathcal{P}}_1(s)\right\rangle$ and $\left\langle\hat{\mathcal{P}}_1(s+\kappa)\right\rangle$:

$$s\left\langle\hat{\mathcal{P}}_m(s)\right\rangle = \gamma_1\left\langle\hat{\mathcal{P}}_1(s)\right\rangle \tag{D9}$$

$$(s+2\kappa)\left\langle\hat{\mathcal{P}}_m(s+2\kappa)\right\rangle = \gamma_1\left\langle\hat{\mathcal{P}}_1(s+2\kappa)\right\rangle. \tag{D10}$$

Finally, we end up with the following equation:

$$\begin{aligned} &\left\langle\hat{\mathcal{P}}_m(s)\right\rangle + f(s)\left\langle\hat{\mathcal{P}}_m(s+2\kappa)\right\rangle \\ &\qquad = \frac{\frac{\omega_R^2}{2}}{(s+2\kappa)\left(s+\kappa+\frac{\tilde{\gamma}}{2}\right)\left(s+\frac{s(\gamma_\mathrm{TL}+s)}{\gamma_1}\right)}, \end{aligned} \tag{D11}$$

with the rational function

$$f(s) \equiv \frac{\frac{\omega_R^2}{2}\left(1+\frac{2s+4\kappa}{\gamma_1}\right)}{s+\frac{s(\gamma_\mathrm{TL}+s)}{\gamma_1}}. \tag{D12}$$

We are interested in the measurement probability in the stationary state, so we want to calculate $\lim_{t\to\infty}\left\langle\hat{\mathcal{P}}_m\right\rangle(t)$. To do so we use relation (C8). Taking the limit on the right hand side of (D12) is straightforward, but the left hand side is more difficult. Taking a closer look at the left hand side we see

$$\begin{aligned} &\lim_{t\to\infty}\mathcal{L}^{-1}\left[\left\langle\hat{\mathcal{P}}_m(s)\right\rangle + f(s)\left\langle\hat{\mathcal{P}}_m(s+2\kappa)\right\rangle\right] \\ &= \underbrace{\lim_{t\to\infty}\mathcal{L}^{-1}\left[\left\langle\hat{\mathcal{P}}_m(s)\right\rangle\right]}_{=\lim_{t\to\infty}\left\langle\hat{\mathcal{P}}_m\right\rangle(t)} \\ &\quad + \underbrace{\lim_{t\to\infty}\int_0^t \mathrm{d}t' f(t')\exp\left[-2\kappa(t-t')\right]\left\langle\hat{\mathcal{P}}_m(t-t')\right\rangle}_{\equiv(*)}. \end{aligned} \tag{D13}$$

The first term gives us the desired limit, while the second one describes a memory kernel that depends on the past of the system.

To solve the integral in (*), we first have to transform $f(s)$ into real space. Since it is a rational function with only first order singularities (the other cases are trivial), $f(t)$ can be calculated using the residue theorem

$$f(t') = \sum_i \alpha_i \exp\left(s_i t'\right), \tag{D14}$$

where s_i are the singularities of the function and α_i the corresponding residues. The singularities are $s_1 = 0$, $s_2 = -(\kappa+\frac{\tilde{\gamma}}{2})$, and $s_3 = -\tilde{\gamma}$. Since $\left\langle\hat{\mathcal{P}}_m(t-t')\right\rangle$ is bounded by one, the limit of the integral is determined by the exponential parts. s_2 and s_3 both damp the integrand; therefore, only the first singularity s_1 gives a contribution to the limit of the integral. As a result, (*) simplifies to

$$\begin{aligned} (*) &= \lim_{t\to\infty}\alpha_1\int_0^t \mathrm{d}t'\exp\left[-2\kappa\left(t-t'\right)\right]\left\langle\hat{\mathcal{P}}_m(t-t')\right\rangle \\ &\overset{(u=t-t')}{=} \alpha_1\int_0^\infty \mathrm{d}u\exp\left[-2\kappa u\right]\left\langle\hat{\mathcal{P}}_m(u)\right\rangle. \end{aligned} \tag{D15}$$

If we evolve $\left\langle\hat{\mathcal{P}}_m(u)\right\rangle$ in a Taylor expansion around zero, we can solve the integral:

$$\begin{aligned} (*) &= \alpha_1\sum_{l=0}^\infty \frac{\left\langle\hat{\mathcal{P}}_m(0)^{(l)}\right\rangle}{l!}\underbrace{\int_0^\infty \mathrm{d}u\exp\left[-2\kappa u\right]u^l}_{=l!(2\kappa)^{-(l+1)}} \\ &= \sum_{l=0}^\infty \frac{\alpha_1}{(2\kappa)^{-(l+1)}}\left\langle\hat{\mathcal{P}}_m(0)^{(l)}\right\rangle, \end{aligned} \tag{D16}$$

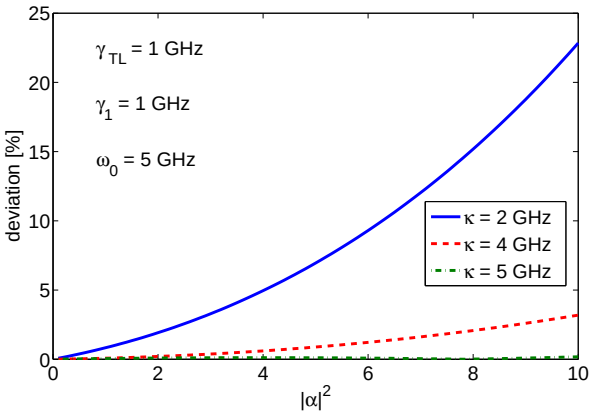

FIG. 8. Comparison between the analytical solution up to fifth order and the numerical solution for the exponentially damped pulse with different values of κ, as a function of $|\alpha|^2$. For small κ and large $|\alpha|^2$ the deviation is quite high, but for increasing κ the approximation fits the numerical results well. For $\kappa = 5$ GHz the deviation is almost zero.

where $\left\langle \hat{\mathcal{P}}_m(0)^{(l)} \right\rangle$ denotes the l th time derivative (at $t = 0$). Calculating the residue

$$\alpha_1 = \lim_{s\to s_1} f(s)(s - s_1) = \frac{\omega_R^2}{2} \frac{1 + 4\frac{\kappa}{\gamma_1}}{\left(\kappa + \frac{\tilde{\gamma}}{2}\right)\left(1 + \frac{\gamma_{\mathrm{TL}}}{\gamma_1}\right)} \tag{D17}$$

and putting this all together in equation (D11), we finally end up with an expression for the measurement probability in the stationary state:

$$\begin{aligned}
\lim_{t\to\infty} \left\langle \hat{\mathcal{P}}_m(t) \right\rangle &= \lim_{s\to 0} \frac{s\frac{\omega_R^2}{2}}{(s + 2\kappa)\left(s + \kappa + \frac{\tilde{\gamma}}{2}\right)\left(s + \frac{s(\gamma_{\mathrm{TL}}+s)}{\gamma_1}\right)} \\
&\quad - \sum_{l=0}^{\infty} \frac{\omega_R^2}{2} \frac{1 + 4\frac{\kappa}{\gamma_1}}{\left(\kappa + \frac{\tilde{\gamma}}{2}\right)\left(1 + \frac{\gamma_{\mathrm{TL}}}{\gamma_1}\right)} \frac{\left\langle \hat{\mathcal{P}}_m(0)^{(l)} \right\rangle}{(2\kappa)^{-(l+1)}} \\
&= \frac{\omega_R^2}{4\kappa\left(\kappa + \frac{\tilde{\gamma}}{2}\right)\left(1 + \frac{\gamma_{\mathrm{TL}}}{\gamma_1}\right)} \\
&\quad - \sum_{l=0}^{\infty} \frac{\omega_R^2}{2} \frac{1 + 4\frac{\kappa}{\gamma_1}}{\left(\kappa + \frac{\tilde{\gamma}}{2}\right)\left(1 + \frac{\gamma_{\mathrm{TL}}}{\gamma_1}\right)} \frac{\left\langle \hat{\mathcal{P}}_m(0)^{(l)} \right\rangle}{(2\kappa)^{-(l+1)}}.
\end{aligned} \tag{D18}$$

The expression up to fifth order has the following form

$$\begin{aligned}
&\lim_{t\to\infty} \left\langle \hat{\mathcal{P}}_m(t) \right\rangle \\
&\quad \approx \frac{\omega_R^2}{4\kappa\left(\kappa + \frac{\tilde{\gamma}}{2}\right)\left(1 + \frac{\gamma_{\mathrm{TL}}}{\gamma_1}\right)} \left(1 - \frac{\omega_R^2}{16\kappa^2}\right).
\end{aligned} \tag{D19}$$

The validity of the approximation up to fifth order is determined by the ratio $\frac{\alpha}{\kappa}$. The smaller this ratio, the better the approximation (see Fig. 8).

[1] J. Clarke and F. K. Wilhelm, Nature **453**, 1031 (2008).
[2] A. Blais, J. Gambetta, A. Wallraff, D. Schuster, S. Girvin, M. Devoret, and R. Schoelkopf, Physical Review A **75**, 032329 (2007).
[3] J. M. Chow, J. M. Gambetta, A. Córcoles, S. T. Merkel, J. A. Smolin, C. Rigetti, S. Poletto, G. A. Keefe, M. B. Rothwell, J. Rozen, *et al.*, Physical review letters **109**, 060501 (2012).
[4] J. Kelly, R. Barends, A. Fowler, A. Megrant, E. Jeffrey, T. White, D. Sank, J. Mutus, B. Campbell, Y. Chen, *et al.*, Nature **519**, 66 (2015).
[5] T. Brecht, W. Pfaff, C. Wang, Y. Chu, L. Frunzio, M. H. Devoret, and R. J. Schoelkopf, arXiv preprint arXiv:1509.01127 (2015).
[6] J. You and F. Nori, Nature **474**, 589 (2011).
[7] M. Hofheinz, H. Wang, M. Ansmann, R. C. Bialczak, E. Lucero, M. Neeley, A. O'Connell, D. Sank, J. Wenner, J. M. Martinis, *et al.*, Nature **459**, 546 (2009).
[8] T. Niemczyk, F. Deppe, H. Huebl, E. P. Menzel, F. Hocke, M. J. Schwarz, J. J. Garcia-Ripoll, D. Zueco, T. Hummer, E. Solano, A. Marx, and R. Gross, Nat Phys **6**, 772 (2010).
[9] A. Baust, E. Hoffmann, M. Haeberlein, M. Schwarz, P. Eder, J. Goetz, F. Wulschner, E. Xie, L. Zhong, F. Quijandria, *et al.*, arXiv preprint arXiv:1412.7372 (2014).
[10] M. Hofheinz, E. Weig, M. Ansmann, R. C. Bialczak, E. Lucero, M. Neeley, A. O?connell, H. Wang, J. M. Martinis, and A. Cleland, Nature **454**, 310 (2008).
[11] B. Vlastakis, G. Kirchmair, Z. Leghtas, S. E. Nigg, L. Frunzio, S. M. Girvin, M. Mirrahimi, M. H. Devoret, and R. J. Schoelkopf, Science **342**, 607 (2013).
[12] G. Kirchmair, B. Vlastakis, Z. Leghtas, S. E. Nigg, H. Paik, E. Ginossar, M. Mirrahimi, L. Frunzio, S. M. Girvin, and R. J. Schoelkopf, Nature **495**, 205 (2013).
[13] C. Wang, Y. Y. Gao, P. Reinhold, R. Heeres, N. Ofek, K. Chou, C. Axline, M. Reagor, J. Blumoff, K. Sliwa, *et al.*, Science **352**, 1087 (2016).
[14] E. Holland, B. Vlastakis, R. Heeres, M. Reagor, U. Vool, Z. Leghtas, L. Frunzio, G. Kirchmair, M. Devoret, M. Mirrahimi, *et al.*, Physical review letters **115**, 180501 (2015).
[15] A. Blais, R.-S. Huang, A. Wallraff, S. M. Girvin, and R. J. Schoelkopf, Phys. Rev. A **69**, 062320 (2004).
[16] S. Krastanov, V. V. Albert, C. Shen, C.-L. Zou, R. W. Heeres, B. Vlastakis, R. J. Schoelkopf, and L. Jiang, Physical Review A **92**, 040303 (2015).
[17] A. Blais, R.-S. Huang, A. Wallraff, S. Girvin, and R. J. Schoelkopf, Physical Review A **69**, 062320 (2004).
[18] L. Sun, A. Petrenko, Z. Leghtas, B. Vlastakis, G. Kirchmair, K. M. Sliwa, A. Narla, M. Hatridge, S. Shankar, J. Blumoff, L. Frunzio, M. Mirrahimi, M. H. Devoret, and R. J. Schoelkopf, Nature **511**, 444 (2014).

[19] B. Abdo, K. Sliwa, L. Frunzio, and M. Devoret, Physical Review X **3**, 031001 (2013).

[20] B. Abdo, K. Sliwa, S. Shankar, M. Hatridge, L. Frunzio, R. Schoelkopf, and M. Devoret, Physical review letters **112**, 167701 (2014).

[21] D. Riste, M. Dukalski, C. Watson, G. De Lange, M. Tiggelman, Y. M. Blanter, K. Lehnert, R. Schouten, and L. DiCarlo, Nature **502**, 350 (2013).

[22] W. F. Kindel, M. Schroer, and K. Lehnert, arXiv preprint arXiv:1510.00663 (2015).

[23] G. Ribeill, D. Hover, Y.-F. Chen, S. Zhu, and R. McDermott, Journal of Applied Physics **110**, 103901 (2011).

[24] D. Hover, Y.-F. Chen, G. Ribeill, S. Zhu, S. Sendelbach, and R. McDermott, Applied Physics Letters **100**, 063503 (2012).

[25] D. Kinion and J. Clarke, Applied Physics Letters **96**, 172501 (2010).

[26] D. Kinion and J. Clarke, Applied Physics Letters **98**, 202503 (2011).

[27] G. G. Claude Cohen Tannoudji, Jacques Dupont-Roc, *Atom-Photon Interactions* (Wiley, Weinheim, 2004).

[28] R. H. Hadfield, Nature photonics **3**, 696 (2009).

[29] L. C. Govia, E. J. Pritchett, S. T. Merkel, D. Pineau, and F. K. Wilhelm, Physical Review A **86**, 032311 (2012).

[30] Y.-F. Chen, D. Hover, S. Sendelbach, L. Maurer, S. Merkel, E. Pritchett, F. Wilhelm, and R. McDermott, Physical review letters **107**, 217401 (2011).

[31] A. Poudel, R. McDermott, and M. G. Vavilov, Physical Review B **86**, 174506 (2012).

[32] G. Romero, J. J. García-Ripoll, and E. Solano, Physical review letters **102**, 173602 (2009).

[33] G. Oelsner, C. Andersen, M. Rehák, M. Schmelz, S. Anders, M. Grajcar, U. Hübner, K. Mølmer, and E. Il'ichev, arXiv preprint arXiv:1605.05935 (2016).

[34] B. Peropadre, G. Romero, G. Johansson, C. Wilson, E. Solano, and J. J. García-Ripoll, Physical Review A **84**, 063834 (2011).

[35] B. Fan, G. Johansson, J. Combes, G. Milburn, and T. M. Stace, Physical Review B **90**, 035132 (2014).

[36] K. Inomata, Z. Lin, K. Koshino, W. D. Oliver, J.-S. Tsai, T. Yamamoto, and Y. Nakamura, arXiv preprint arXiv:1601.05513 (2016).

[37] C. H. Wong and M. G. Vavilov, arXiv preprint arXiv:1512.06939 (2015).

[38] L. C. Govia, E. J. Pritchett, C. Xu, B. Plourde, M. G. Vavilov, F. K. Wilhelm, and R. McDermott, Physical Review A **90**, 062307 (2014).

[39] L. C. Govia, E. J. Pritchett, B. Plourde, M. G. Vavilov, R. McDermott, and F. K. Wilhelm, Physical Review A **92**, 022335 (2015).

[40] K. Koshino, K. Inomata, T. Yamamoto, and Y. Nakamura, Physical review letters **111**, 153601 (2013).

[41] K. Koshino, K. Inomata, Z. Lin, Y. Nakamura, and T. Yamamoto, Physical Review A **91**, 043805 (2015).

[42] K. Koshino, Z. Lin, K. Inomata, T. Yamamoto, and Y. Nakamura, Physical Review A **93**, 023824 (2016).

[43] D. M. Pozar, *Microwave Engineering* (Wiley, New Jersey, 2012).

[44] G. Romero, J. J. García-Ripoll, and E. Solano, Physica Scripta **2009**, 014004 (2009).

[45] C. Gardiner and M. Collett, Physical Review A **31**, 3761 (1985).

[46] A. Clerk, M. Devoret, S. Girvin, F. Marquardt, and R. Schoelkopf, Reviews of Modern Physics **82**, 1155 (2010).

[47] J. M. Martinis, M. H. Devoret, and J. Clarke, Physical review letters **55**, 1543 (1985).

[48] K. Likharev and A. Zorin, Journal of Low Temperature Physics **59**, 347 (1985).

[49] M. R. Geller, E. J. Pritchett, A. T. Sornborger, and F. Wilhelm, in *Manipulating Quantum Coherence in Solid State Systems* (Springer, 2007) pp. 171–194.

[50] J. Johansson, G. Johansson, C. Wilson, and F. Nori, Physical Review A **82**, 052509 (2010).

[51] D. Walls and G. J. Milburn, *Quantum Optics* (Springer, Heidelberg, 2008).

[52] E. T. Jaynes and F. W. Cummings, Proceedings of the IEEE **51**, 89 (1963).

[53] C. W. Gardiner and P. Zoller, *Quantum Noise* (Springer, Heidelberg, 2004).

[54] H. P. Breuer and F. Petruccione, *The Theory of Open Quantum Systems* (Oxford university press, Oxford, 2010).

[55] M. Göppl, A. Fragner, M. Baur, R. Bianchetti, S. Filipp, J. Fink, P. Leek, G. Puebla, L. Steffen, and A. Wallraff, Journal of Applied Physics **104**, 113904 (2008).

[56] A. Megrant, C. Neill, R. Barends, B. Chiaro, Y. Chen, L. Feigl, J. Kelly, E. Lucero, M. Mariantoni, P. O'Malley, *et al.*, Applied Physics Letters **100**, 113510 (2012).

[57] B. Q. Baragiola, R. L. Cook, A. M. Brańczyk, and J. Combes, Physical Review A **86**, 013811 (2012).

[58] J. Zmuidzinas, Applied optics **42**, 4989 (2003).

[59] R. Thornton, P. Ade, S. Aiola, F. Angile, M. Amiri, J. Beall, D. Becker, H. Cho, S. Choi, P. Corlies, *et al.*, arXiv preprint arXiv:1605.06569 (2016).

[60] D. Flanigan, H. McCarrick, G. Jones, B. R. Johnson, M. Abitbol, P. Ade, D. Araujo, K. Bradford, R. Cantor, G. Che, *et al.*, Applied Physics Letters **108**, 083504 (2016).

[61] Ş. E. Kocabaş, E. Rephaeli, and S. Fan, Physical Review A **85**, 023817 (2012).

[62] J. Wenner, Y. Yin, Y. Chen, R. Barends, B. Chiaro, E. Jeffrey, J. Kelly, A. Megrant, J. Mutus, C. Neill, *et al.*, Physical Review Letters **112**, 210501 (2014).